ELSEVIER

Contents lists available at ScienceDirect

### **Applied Surface Science**

journal homepage: www.elsevier.com/locate/apsusc



## Tailoring the sodium doped LiMnPO<sub>4</sub>/C orthophosphate to nanoscale as a high-performance cathode for lithium ion battery



Jun Zhang<sup>a,\*</sup>, Shao-Hua Luo<sup>b,c,d</sup>, Qun-Xiang Ren<sup>a</sup>, Da-Jun Zhang<sup>a</sup>, Yan Qin<sup>a</sup>

- <sup>a</sup> College of Basic Medical Sciences, Shenyang Medical College, Shenyang 110034, People's Republic of China
- b School of Resources and Materials, Northeastern University at Qinhuangdao, Qinhuangdao 066004, People's Republic of China
- <sup>c</sup> Key Laboratory of Dielectric and Electrolyte Functional Material Hebei Province. Oinhuanedao 066004. People's Republic of China
- d School of Materials Science and Engineering, Northeastern University, Shenyang 110004, People's Republic of China

#### ARTICLE INFO

# Keywords: Lithium-ion battery LiMnPO<sub>4</sub> Sodium ions doping Core-shell structure Electrochemical performance

#### ABSTRACT

Three-dimensional nanoscale LiMnPO $_4$ /C orthophosphate with sodium ion substitution in Li site has successfully synthesized by a facile hydrothermal method, using precipitated Li $_{3-x}$ Na $_x$ PO $_4$  hollow microspheres as the sacrificial templates. Meanwhile, Li $_3$ PO $_4$  impurity phase is generated. The chemical/physical properties are characterized by X-ray diffraction (XRD), scanning electron microscope (SEM), transmission electron microscopy (TEM), Brunauer-Emmett-Teller (BET), the charge-discharge method, cyclic voltammetry (CV) and electrochemical impedance spectroscopy (EIS), and the effects of Li $_3$ PO $_4$  on structure and electrochemical performance have been investigated. In particular, the existence of Li $_3$ PO $_4$  and proper sodium ions doping is beneficial to stabilize crystal structure and assemble into three-dimensional porous core-shell structure, aiming to provide abundant channels and active sites for accelerating lithium ion migration rate. Compared with other samples, the Li $_{0.9}$ Na $_{0.1}$ MnPO $_4$ /C composite demonstrates the excellent electrochemical performance, which delivers the first specific discharge capacity of 152 mAh/g at 0.05 C with little capacity fading after 200 cycles. The discharge capacity still maintains at 122.3 mAh/g, even at a rate of 10 C. Our experiments indicate that the synergetic effect of sodium doping and the formed three-dimensional porous core-shell structure provide high rate capability and cycle performance.

#### 1. Introduction

Lithium-ion batteries (LIBs) are recognized as one of the most promising energy storage devices due to the high energy and power densities, especially for the development of powering electric vehicles (EVs) and hybird electric vehicles (HEVs) in the predictable future [1–7]. The sustainable growing demands of higher energy/power densities and structural stability for LIBs are critically depended on the electrochemical properties of cathode materials. In this regard, polyanion-type LiMnPO<sub>4</sub> has become prospective storage cathode candidate material due to the advantages of high energy density (700 Wh/kg), high structural stability, low cost and good environmental compatibility [8–10]. Hence, the electrochemcial window of LiMnPO<sub>4</sub> matches well with the current organic carbonate electrolytes. However, the low intrinsic electronic and ionic conductivity of LiMnPO<sub>4</sub> greatly restrict lithium ions motion rate passing through two-phase interface and seriously hinder the commercialization application [11,12]. To ameliorate the electrochmcial performance of LiMnPO<sub>4</sub>/C, the modification of polyanionic-based LiMnPO<sub>4</sub>/C composites materials have been widely studied in the past decades, especially in the aspect of tailoring particles size [13-15], doping metal ions [16-25,30-31] and coating conductive materials (carbon, metal/metal oxides or conducting polymer) [26,27]. In general, tailoring particles and achieving nanosized particles is especially important for the electrochemical properties in LiMnPO<sub>4</sub>/C. Recently, nano-pyramid like LiMnPO<sub>4</sub>/C material has delivered the first discharge capacity of 164.2 mAh/g and retained the capacity of 130.8 mAh/g up to 500th cycle at 0.1 C [13], the results showed that nanopyramid like morphology increases the lithium diffusion kinetics and conductivity, thus achieving excellent electrochemical performance. Kwon et al. [15] investigated the influences of diverse shapes of LiMnPO<sub>4</sub> nanoparticles, like an elongated spherical, thin nano-rod, thick nano-rod, cubic and platelet shapes on the tap densities, the path and the direction of Li<sup>+</sup> diffusion systematically, the performance improvement could be ascribed to the high surface area and short lithium ion diffusion path in nanosized LiMnPO<sub>4</sub>. Therefore, the strategy of tailoring the particles size can effectively enhance the performance of

<sup>\*</sup>Corresponding author at: Shenyang Medical College, 110034, People's Republic of China. E-mail address: junjun376@163.com (J. Zhang).

Applied Surface Science 530 (2020) 146628

materials by enlarging the lithium ions diffusion channels. Unfortunately, there is a common unavoidable shortcoming that the nanosized active materials tend to reunite and show poor electrochemical activity.

To address the problem, the approaches of cations doping to enhance the ionic diffusion rate have been researched [28,29]. So far, doping of LiMnPO<sub>4</sub> on Mn site by various cations are often reported to enhance the electrochemcial performance. However, there still have some researches take a different view that doping heterovalent ions at Mn site would obstruct the lithium ions diffusion channels, leading to low ionic conductivity activity. For the case of the manganese-based olivine material, several attempts have reported the partial substitution of lithium by metal ions in order to build abundant point defect to regulate the electronic structure, and improve the electrochemical performance of the cathode material. In addition, sodium is earthabundant element and has the similar electronic structure and properties as lithium. The introduce of sodium ions in the lattice position could change the band structure between valence band and conduction band, and possibly increase the interlayer space for facile lithium movement during intercalation and deintercalation process. Previously, Redouan et al. [19] and Rajammal et al. [21] have proposed minor molar ratios of Na+ to substitute Li+ in the solid-solution  $\text{Li}_{1-x}\text{Na}_x\text{MPO}_4$  (M = Fe, Mn) (0  $\leq$  x  $\leq$  0.05) phase, and revealed the influence of sodium-incorporated lithium manganese phosphate as an active material on its performance in electrochemical study for energy storage application. Meanwhile, Chen et al. [22] investigated the appropriate charge compensation mechanisms of Li<sub>1-x</sub>Al<sub>x</sub>MnPO<sub>4</sub>, the results suggest that Al3+ can be doped into the lattice of LiMnPO4 and the preferable doping mechanism is Al<sup>3+</sup> occupies Li<sup>+</sup> site with charge compensation by electronic defect, which is helpful to better understand the aliovent doping behavior in LiMnPO<sub>4</sub>. The charge-compensation mechanism is much different from those previously reported and needs further study. Nowadays, lithium storage materials of sodium doping at Li site has been extensively investigated for the materials of  $\text{Li}_3\text{V}_2(\text{PO}_4)_3$  [32–35],  $\text{Li}_{1-x}\text{Na}_x\text{FePO}_4$  [36], and confirmed the overall conductivity and excellent electrochemical performance. There have numerous studies on lithium-sodium hybrid battery, which provides suggestion for the design new energy storage materials in the future. The lithium-sodium hybrid ion NaLi<sub>2</sub>V<sub>2</sub>(PO<sub>4</sub>)<sub>3</sub>/C with rhombohedral phase were synthesized by Jia et al. [32], the corresponding first-cycle capacities reached 124.8 and 130 mAh/g. The appropriate lithium-sodium ratios showed better Li storage properties than previously reported specimens, and were concluded to be promising Li storage materials. Zuo et al. [33] synthesized  $\rm Li_{2.6}Na_{0.4}V_2(PO_4)_3/C$  composite with a high energy density of 478.8 Wh/kg, which further proved sodium doping can stabilize the rhombohedral structure of the V2(PO4)3 framework, leading to the remarkable cycling stability. Although many systematical researches have attempted to understand the changes of lithium/sodium co-existing storage behaviors and the inner mechanisms of the performance improvement in olivine-type phase, the specific mechanisms of electrochemical inactive sodium ion substitution on the Li site in the LiMnPO<sub>4</sub> material has still been unclear until now.

In the present study, in order to improve the intrinsic electronic and ionic transport properties, we focus on the sodium ions substitution of LiMnPO $_4$  at Li site and constructing a core-shell structure nanosized LiMnPO $_4$  to facilitate the reaction kinetics and stabilize the crystal structure for improving the electrochemical performance. Herein, we report a co-precipitation process to synthesize hollow microspheres  ${\rm Li}_{3-x}{\rm Na}_x{\rm PO}_4$  as the sacrificial templates, subsequently design a facile hydrothermal approach to prepare the core-shell structure  ${\rm Li}_{1-x}{\rm Na}_x{\rm MnPO}_4/{\rm C}$  composite cathode. Furthermore, the influences of decorated structure, template size and sodium doped contents on the phase structure, products size and electrochemical characteristics of  ${\rm Li}_{1-x}{\rm Na}_x{\rm MnPO}_4/{\rm C}$  electrode are systematically investigated to evaluate its future applicability as a cathode for lithium-ion battery.

#### 2. Experimental

#### 2.1. Preparation of materials

 ${\rm Li_{1-x}Na_xMnPO_4/C}$  (x = 0, 0.05, 0.1, 0.15, 0.2, 0.3) composites were prepared by a simple hydrothermal approach using MnSO<sub>4</sub>·H<sub>2</sub>O, hollow  ${\rm Li_{3-x}Na_xPO_4}$  as raw materials. The  ${\rm Li_{3-x}Na_xPO_4}$  (x = 0, 0.15, 0.3, 0.45, 0.6, 0.9) precursors were synthesized by dropping a certain concentration of 85% H<sub>3</sub>PO<sub>4</sub> (50 ml) solution into different molar ratio LiOH/NaOH aqueous mixture solution (200 ml) using the peristaltic pump under a certain flowing rate at bathing temperature of 50, in which the molar ratio of Li:Na:P was 3-x:x:1. Then, the white powders were started to nucleate and form gradually with vigorous stirring. Then, the  ${\rm Li_{3-x}Na_xPO_4}$  precursors were generated after filtered, washed with distilled water and dried at 80 °C in air atmosphere.

The synthesis process of  $\rm Li_{1-x}Na_xMnPO_4/C$  composites were illustrated as follows. The aqueous solution of  $\rm MnSO_4\cdot H_2O$  (99%) and  $\rm Li_{3-x}Na_xPO_4$  precursor were slowly added in a molar ratio of 1:1, followed by the addition of a certain amount ascorbic solution in 36 ml of PEG400-H<sub>2</sub>O mixture solvents (v/v = 1:2) under vigorous stirring. In this way, the sodium doped LiMnPO<sub>4</sub>/C precursors were formed and surrounded by porous conductive carbon layer. The resulting mixture was sealed in a 50 ml Teflon-lined autoclave and reacted at 160 °C for 9 h to form the  $\rm Li_{1-x}Na_xMnPO_4/C$  precursors. The pure  $\rm Li_{1-x}Na_xMnPO_4/C$  precursors were generated after centrifuged, washed, and dried at 80 °C a few hours. Finally, the  $\rm Li_{1-x}Na_xMnPO_4/C$  composites were gained by calcining at 550 °C for 3 h under  $\rm N_2$  atmosphere.

#### 2.2. Material characterization

The crystal data were gathered by the Rigaku Smartlab X-ray diffraction instrument (XRD) with Cu K $\alpha$  radiation ranging from 10 to 80 at a scan rate of 2.4 /min. The microscopic structure and element distribution were examined by the ZEISS SUPRA55 scanning electron microscopy (SEM) and JEOL JEM2100F transmission electron microscope (TEM). The specific surface area value was measured by the Brunauer-Emmett-Teller method (BET) using SSA-4300 instrument.

#### 2.3. Electrochemical measurements

The electrochemical parameters of Li<sub>1-x</sub>Na<sub>x</sub>MnPO<sub>4</sub>/C cathode materials were recorded by two electrode system, liking CR2032 button cells, which was fabricated in high purity Ar-filled glove box. The cathode was obtained by blending active materials, acetylene and PVDF in NMP solvent in a mass proportion of 8:1:1 with continuously stirring for at least 1 h to ensure the uniformity of the mixture. The mixture was pasted on the Al foil and dried for 10 h at 80 and 120 °C in open conditions and under vacuum, respectively. The coated Al foil was rolled and pressed into wafer for cell assembled with the area of 0.785 cm<sup>2</sup>. In the testing system, lithium plate was used as anode electrode, Celgard 2400 and 1 M LiPF $_6$ /EC + DEC + MEC (v/v/ v = 1:1:1) mixture was used as membrane and the electrolyte. The galvanostatic charge-discharge tests were measured using the Land CT2001A battery testing systems with the voltage range of 2.5-4.5 V under different rates. The electrochemical impedance spectroscopy (EIS) and cyclic voltammetry (CV) were tested on a Solartron 1260 + 1287 electrochemical impedance analyzer. The testing frequency of EIS were ranging from 105 Hz to 0.1 Hz with the voltage amplitude of 10 mV. The voltage interval of CV was 2.5-4.5 V at a scan rate of 0.1 mV/s. All tests were conducted at room temperature.

#### 3. Results and discussion

A series of  $Li_{3-x}Na_xPO_4$  precursors (x = 0, 0.15, 0.3, 0.45, 0.6, 0.9) are synthesized by co-precipitation process and phase structures of the

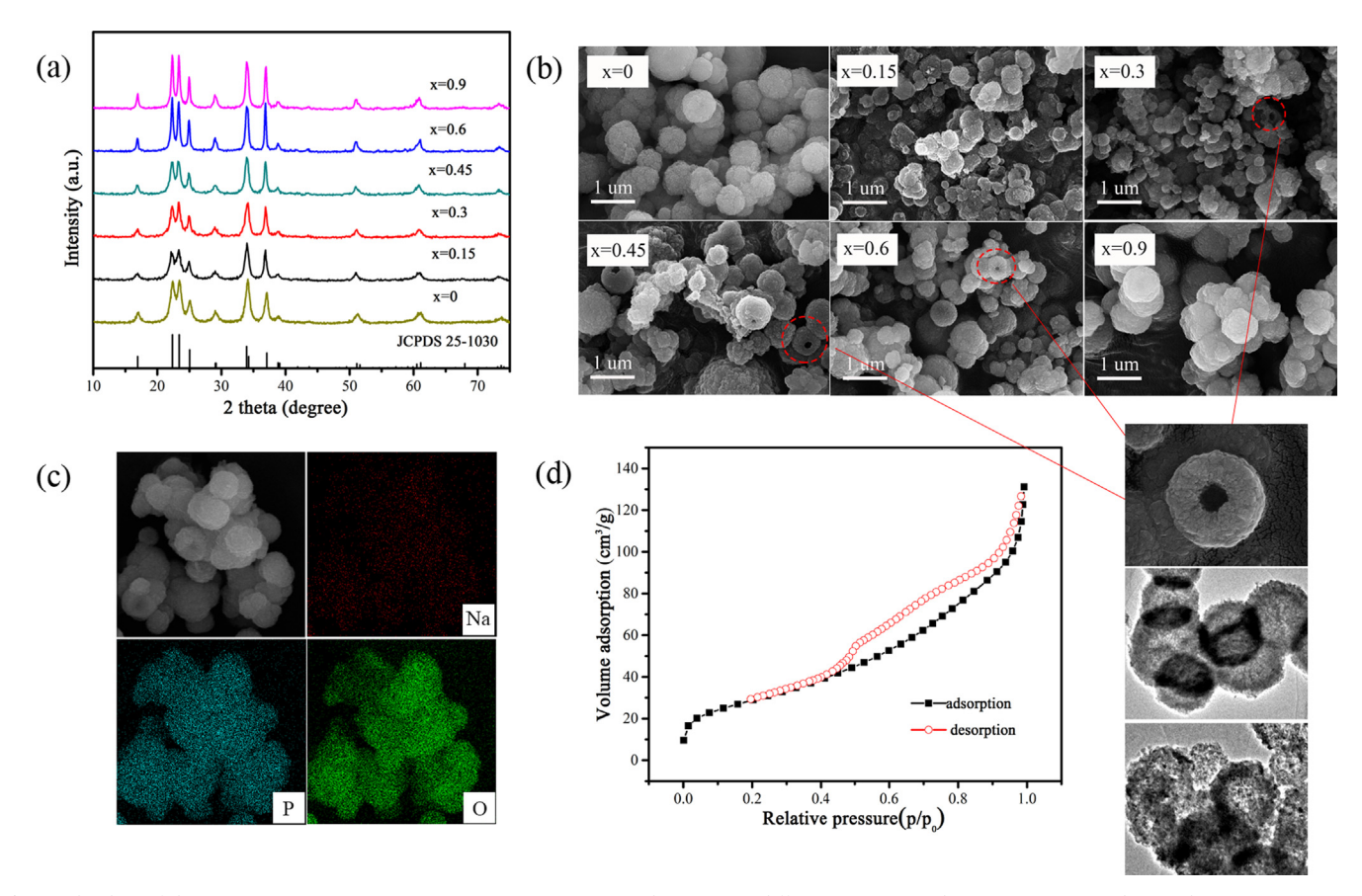


Fig. 1. The data of the  $\text{Li}_{3-x}\text{Na}_{x}\text{PO}_{4}$  (x=0,0.15,0.3,0.45,0.6,0.9) samples: (a) XRD diffraction patterns, (b) SEM images, (c) Elemental mapping patterns of  $\text{Li}_{2.7}\text{Na}_{0.3}\text{PO}_{4}$ , (d) Nitrogen adsorption-desorption isotherms of  $\text{Li}_{2.7}\text{Na}_{0.3}\text{PO}_{4}$  prepared by precipitation method.

precursors are studied by XRD. As shown in Fig. 1a, the X-ray diffraction peaks of Li3-xNaxPO4 precursors are well corresponding to the single phase lithium phosphate standard card JCPDS 25-1030, indicating that the high purity and crystallization of the obtained precursors. No impurity phase peak is detected, which means the doping amounts of sodium ions have no influence on the crystalline structure of Li<sub>3-x</sub>Na<sub>x</sub>PO<sub>4</sub> precursors. In addition, Li<sub>2.7</sub>Na<sub>0.3</sub>PO<sub>4</sub> sample shows the relatively weak and wide diffraction peaks compared with other samples, illustrating that Li<sub>2.7</sub>Na<sub>0.3</sub>PO<sub>4</sub> has the smaller grain size. The morphology and microstructure of Li<sub>3-x</sub>Na<sub>x</sub>PO<sub>4</sub> precursors (x = 0, 0.15, 0.3, 0.45, 0.6, 0.9) are characterized by SEM and the recording images are shown in Fig. 1b. As we can see, the Li<sub>3-x</sub>Na<sub>x</sub>PO<sub>4</sub> precursors display hollow-porous spherical structure particles (as shown in red dashed circle), and the grain diameters vary with the adding amounts of sodium ions. Compared with other samples, when the adding percentage of sodium/lithium ion is 10% (i.e. x = 0.3), the sample appears relatively small diameter range (150-300 nm) and high specific area, slight agglomeration is also observed. Once exceeding the certain percentage, the average diameter of particles keep growing, and agglomeration phenomenon become more serious, which are consist with the variation trend of XRD. The results indicate that the addition of sodium ions could hinder the growth of Li<sub>3</sub>PO<sub>4</sub> grains within the sodium/lithium ratio of 10%, leading to obvious decrease of grain sizes, but excessive sodium ions could cause the growth of particle diameters as well. To ensure the presence of sodium ions in the Li2.7Na0.3PO4 powder, the elemental mapping patterns are conducted and the results are presented in Fig. 1c. It is observed that sodium element distributes uniformly in the Li<sub>2.7</sub>Na<sub>0.3</sub>PO<sub>4</sub> sample. The specific surface area of Li<sub>2.7</sub>Na<sub>0.3</sub>PO<sub>4</sub> precursor can be obtained by the nitrogen adsorptiondesorption isotherms (Fig. 1d) and the value is 84.60 m<sup>2</sup>/g, which is higher than the pure  $\text{Li}_3\text{PO}_4$  (79.19 m<sup>2</sup>/g) [37]. The hollow structure

and high specific area  $\rm Li_{2.7}Na_{0.3}PO_4$  precursor used as the sacrificial templates could provide larger reaction interface for the preparation of nanosized  $\rm Li_{1-x}Na_xMnPO_4/C$  materials, and further influence its intrinsic and electrochemical properties.

As illustrated above, different amounts of sodium doped LiMnPO<sub>4</sub>/C composites are formed through the subsequent hydrothermal method. After calcination, a series of sodium doped  $Li_{1-x}Na_xMnPO_4/C$  (x = 0, 0.05, 0.1, 0.15, 0.2, 0.3) nanoparticles are obtained. The crystal phase structures of the as-prepared samples are investigated by XRD and the corresponding patterns are displayed in Fig. 2a. The diffraction patterns show many sharp peaks, all the main diffraction peaks are well index with the defined olivine structure LiMnPO<sub>4</sub> (JCPDS card No. 33-0803) with the space group of Pnma, indicating the high purity and crystallinity of the as-synthesized samples. To further understand the effects of sodium ions doping, we calculate all the diffraction patterns by High Score Software, and the Riteveld lattice parameters and grain sizes of  $\text{Li}_{1-x}\text{Na}_x\text{MnPO}_4/\text{C}$  (x = 0, 0.05, 0.1, 0.15, 0.2, 0.3) samples are listed in Table 1. Obviously, the lattice parameters a, b, c and the cell volume enlarge slightly with the continuous adding contents, proving the successfully doping of sodium ions in the LiMnPO<sub>4</sub> lattice. Furthermore, the detail view in the range of 25.0–25.6° is shown in Fig. 2b. It is worth mentioning that the (1 1 1) peak slightly shifts to the small angles with the increasing contents of sodium ions, which may lead to the formation of Li<sub>1-x</sub>Na<sub>x</sub>MnPO<sub>4</sub>/C continuous solid solutions, and further proves sodium ions have perfectly entered into the host lattice. It is well known that the ionic radius of sodium ions (0.098 nm) is larger than that of lithium ions (0.076 nm), some changes in the lattice distances and crystal volume could occur due to sodium ions doping. As a result, a distortion of the lattice and an increase in the total volume are obtained with the insertion of sodium ions. No carbon peaks are detected and proved the existence of amorphous residual carbon in the bulk

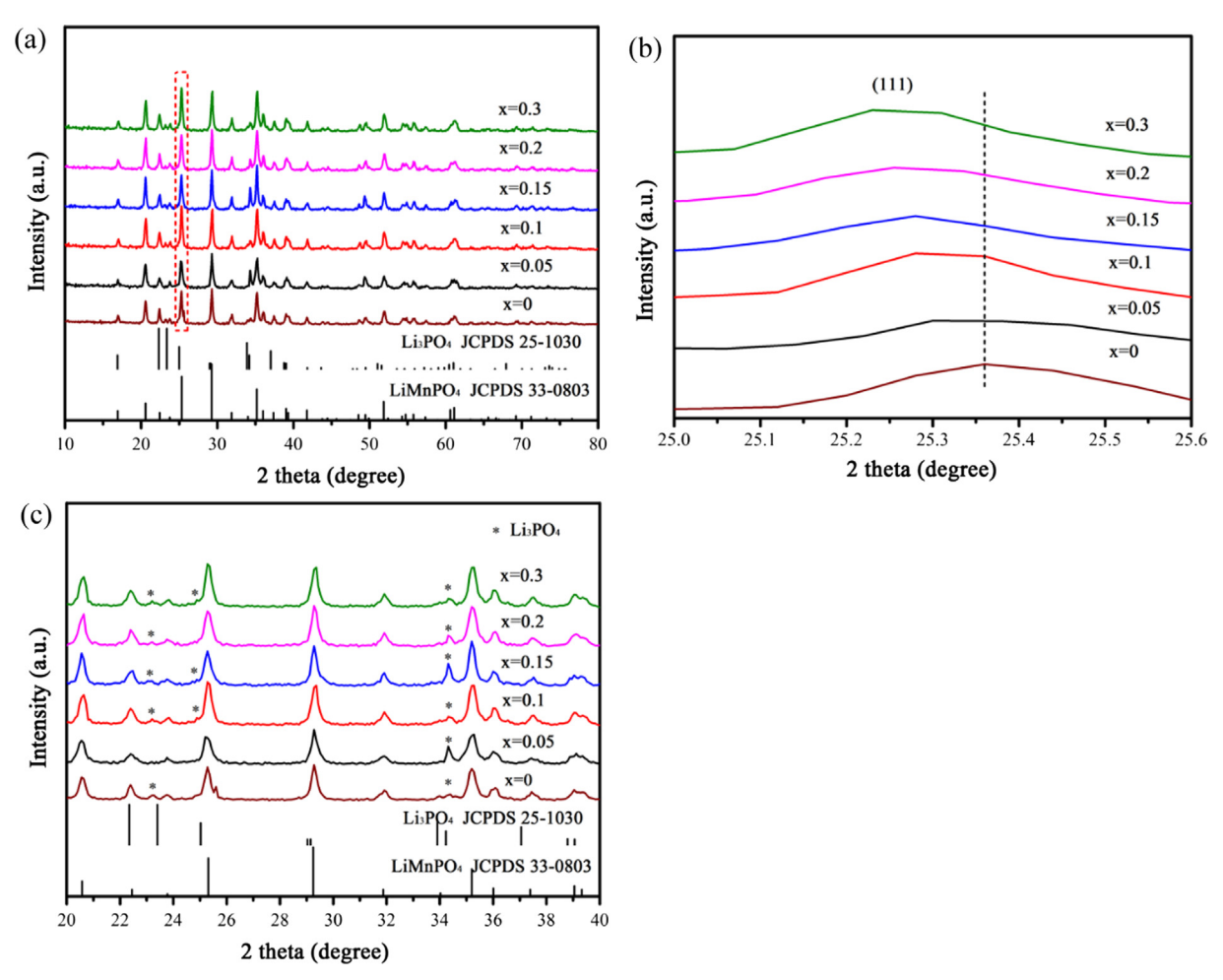


Fig. 2. (a) XRD diffraction patterns of the  $\text{Li}_{1-x}\text{Na}_x\text{MnPO}_4/\text{C}$  (x = 0, 0.05, 0.1, 0.15, 0.2, 0.3); (b, c) partially magnified angles of 25–25.6° and 20–40°.

Table 1 Rietveld refinement lattice parameters of the  ${\rm Li}_{1-x}{\rm Na}_x{\rm MnPO}_4/{\rm C}$  (x = 0, 0.05, 0.1, 0.15, 0.2, 0.3) samples.

| Samples   | a/Å  | b/Å   | c/Å  | Volume/Å <sup>3</sup>                          |
|---|--|---|--|--|
| x = 0 $x = 0.05$ $x = 0.1$ $x = 0.15$ $x = 0.2$ | 4.7418<br>4.7432<br>4.7469<br>4.7483<br>4.7498 | 10.4445<br>10.4456<br>10.4473<br>10.4492<br>10.4511 | 6.1018<br>6.1029<br>6.1047<br>6.1061<br>6.1077 | 302.37<br>302.57<br>302.78<br>303.06<br>303.28 |
| x = 0.3   | 4.7520   | 10.4573   | 6.1098   | 303.64   |

materials. Some additional tiny diffraction peaks labeled with the symbol "\*" are corresponding to the  $\rm Li_3PO_4$  impurity phase (JCPDS card No. 25-1030) (Fig. 2c), revealing that different sodium contents obviously affect the formation of  $\rm Li_3PO_4$ . The generated hollow-porous  $\rm Li_3PO_4$  nanoparticles mixing in the phosphate polyanionic cathode material play an important role in increasing the specific surface area for the adequate contact area with the electrolyte, and further improve the lithium ions diffusion rate and decrease the charge transfer resistances.

To understand the effects of sodium ions amounts used in the synthesis of LiMnPO<sub>4</sub> on morphology and nanostructure, the SEM analysis is carried out on the sodium doped Li<sub>1-x</sub>Na<sub>x</sub>MnPO<sub>4</sub>/C (x = 0, 0.05, 0.1, 0.15, 0.2, 0.3) samples, and the photographs are shown in Fig. 3. All the samples appear as semblable surface morphologies, composing of dense and irregular spherical-like shape agglomerated nano-grains. With the increasing of sodium ions amounts, tremendous porous channels and separate spheres are generated. The continuous

adding of sodium ions, the particle agglomeration problem get worse. The formation of particles aggregation would lead to poor lithium ions storage performance. The grain size (D) of  $Li_{1-x}Na_xMnPO_4/C$  (x = 0, 0.05, 0.1, 0.15, 0.2, 0.3) can be calculated by the Scherrer equation  $D = \frac{K\lambda}{\beta\cos\theta}$ , where K is the Scherrer constant (K = 0.94),  $\lambda$  is the X-ray wavelength,  $\beta$  is the full width at half maximum of the peak,  $\theta$  is the angle of diffraction. With sodium ions contents increasing, the average grain sizes are calculated to be 69 nm, 42 nm, 48 nm, 87 nm, 158 nm, 249 nm, respectively. It is observed that the sample with sodium/lithium ratio of 10% displays better monodispersity, uniform distribution and high porosity, suggesting an appropriate amounts of sodium ions doping can prevent the grains growing and enlarge the contact interface area between the nano-grains and electrolyte. These may be due to the porous structure could hinder the particles from agglomeration, meanwhile the porous channels are tens of nanometers width that most of them allow lithium ions pass through the bulk material efficiently, which ultimately enhance the electrochemical performance. For qualitative analysis, the elemental mappings of Li<sub>0.9</sub>Na<sub>0.1</sub>MnPO<sub>4</sub>/C are tested and shown in Fig. 4. All the pictures confirm that Na, Mn, P and O elements are distributed homogeneously all through the Li<sub>0.9</sub>Na<sub>0.1</sub>MnPO<sub>4</sub>/C sample as expected, the exsistence of sodium ions are also clearly observed from the images. Even though elemental mappings are not accurately characterization method, but the observed qualitative results are acceptable.

For further observation the interior structure of the as-prepared samples, HRTEM technique is adopted and the relevant images of  $\text{Li}_{0.9}\text{Na}_{0.1}\text{MnPO}_4/\text{C}$  are shown in Fig. 5. Fig. 5a–c depict that numerous  $\text{Li}_{0.9}\text{Na}_{0.1}\text{MnPO}_4/\text{C}$  nanosized grains pile together and form slightly

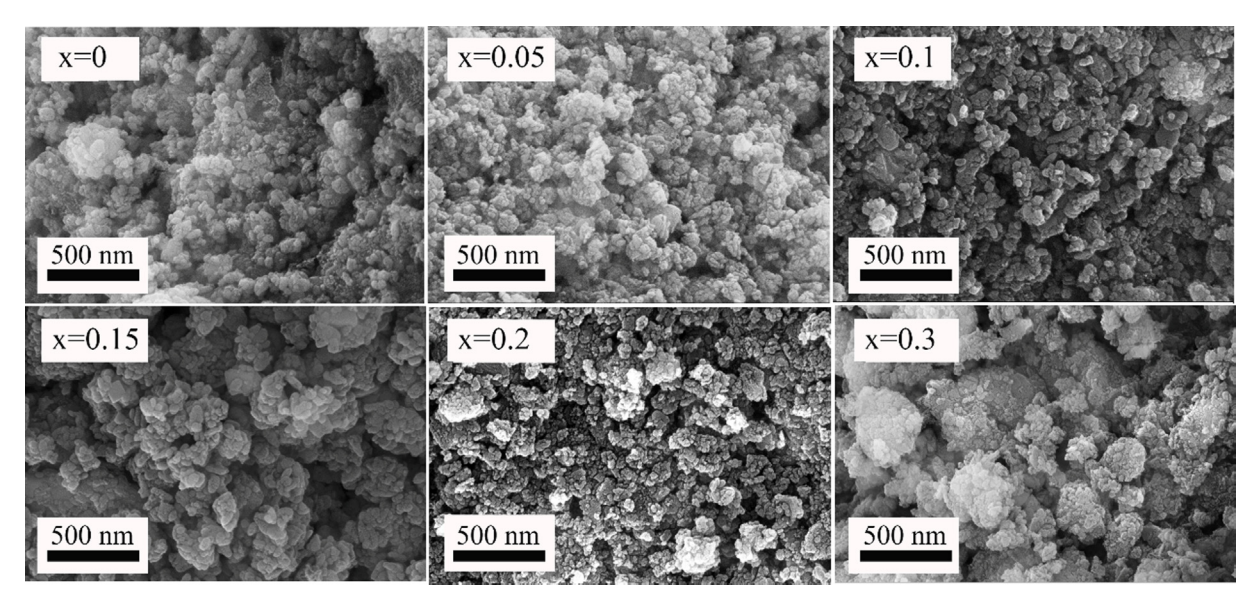


Fig. 3. SEM micrographs of the  $\text{Li}_{1-x}\text{Na}_x\text{MnPO}_4/\text{C}$  samples: (a) x=0, (b) x=0.05, (c) x=0.1, (d) x=0.15, (e) x=0.2, (f) x=0.3.

agglomeration, the grain sizes are ranging from 30 to 70 nm, and the results are in line with the SEM images. Obviously, the  $\rm Li_{0.9}Na_{0.1}MnPO_4/C$  is surrounded by the carbon layer uniformly (Fig. 5b, the red arrow), and form the core-shell structure. In Fig. 5d, it is observed that the unregular carbon layer with thickness of 4–6 nm coated on the surface can provide a good conductive network for good electrochemical activity of the material. The above overall analysis of microstructure and morphology features have indicated that the sodium doped LiMnPO<sub>4</sub>/C with nanosized porous structure has been prepared successfully. The porous structure and interconnected cellular apparent state could validly improve the electrochemical activity of sodium doped LiMnPO<sub>4</sub>/C, due to the adequate contact interface between the electrolyte and the target material.

The galvanostatic charge-discharge curves of  ${\rm Li_{1-x}Na_xMnPO_4/C}$  (x = 0, 0.05, 0.1, 0.15, 0.2, 0.3) electrodes are measured at 0.05 C rate under room temperature and the results are displayed in Fig. 6. All the samples show a flat discharge plateaus at approximately 4.0 V (vs. Li/Li<sup>+</sup>), which correspond to the two phase redox process between the

Mn<sup>3+</sup>/Mn<sup>2+</sup> redox couple. It is obviously observed that the adding amounts of sodium ions influence the specific capacities of LiMnPO<sub>4</sub>/C greatly. With the adding amounts increasing, the discharge capacities increase first and then decrease with a peak value appearing. Compared with other samples, the  $\text{Li}_{0.9}\text{Na}_{0.1}\text{MnPO}_4/\text{C}$  electrode delivers the highest initial discharge capacity of 152 mAh/g at 0.05 C rate. The improvement of specific capacity is attributed to the increased reaction sites for lithium ion intercalation/deintercalation with a moderate amounts of sodium ions. Fig. 6 also shows the voltage profiles of the asprepared samples, the columbic efficiency of  $\text{Li}_{1-x}\text{Na}_x\text{MnPO}_4/\text{C}$  (x = 0, 0.05, 0.1, 0.15, 0.2, 0.3) composites are calculated to be 72.26%, 78.67%, 89.97%, 77.24%, 76.11%, 85.36%, respectively. Among all the samples, Li<sub>0.9</sub>Na<sub>0.1</sub>MnPO<sub>4</sub>/C appears slightly increased columbic efficiency. The voltage difference between charge and discharge profiles are 194.4 mV, 167.1 mV, 165.3 mV, 168.4 mV, 171.5 mV, 253.8 mV, respectively, demonstrating that Li<sub>0.9</sub>Na<sub>0.1</sub>MnPO<sub>4</sub>/C has excellent reaction process kinetics and low polarization due to the enhanced electron conductivity and lithium ion diffusion rate.

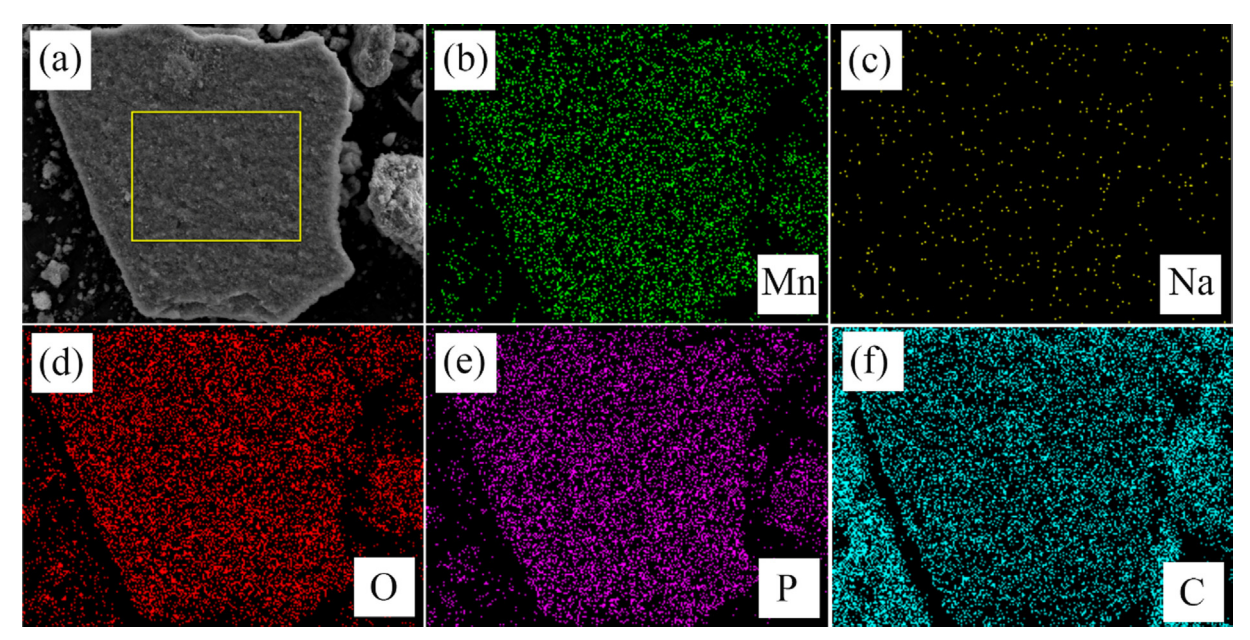


Fig. 4. Elemental mappings of Li<sub>0.9</sub>Na<sub>0.1</sub>MnPO<sub>4</sub>/C.

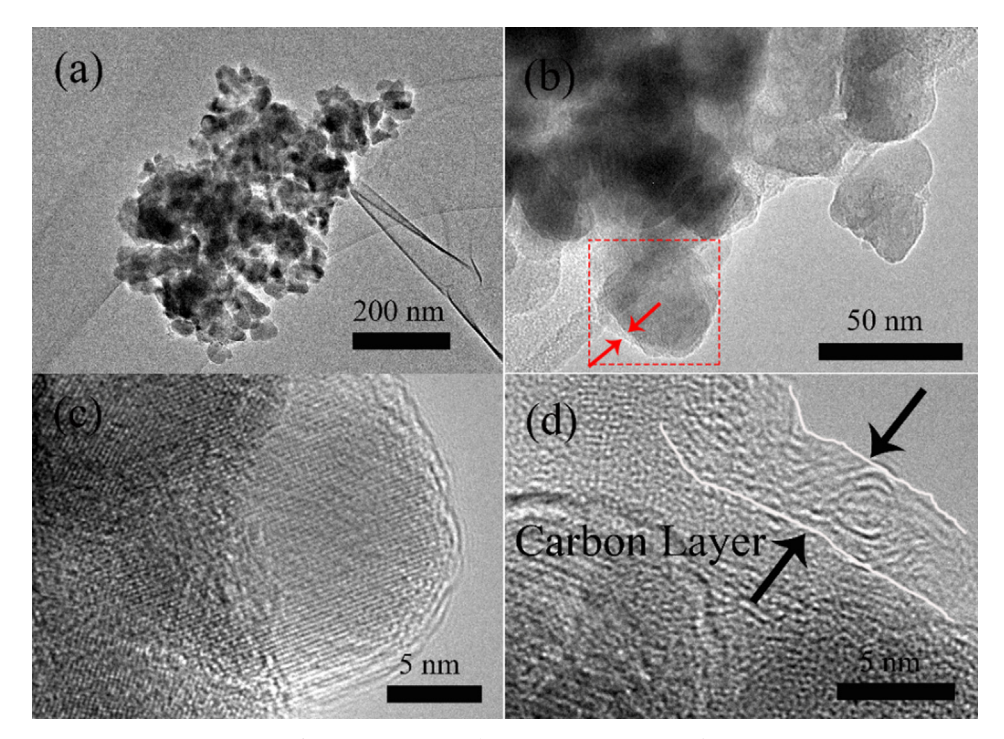


Fig. 5. TEM images of  $Li_{0.9}Na_{0.1}MnPO_4/C$  sample.

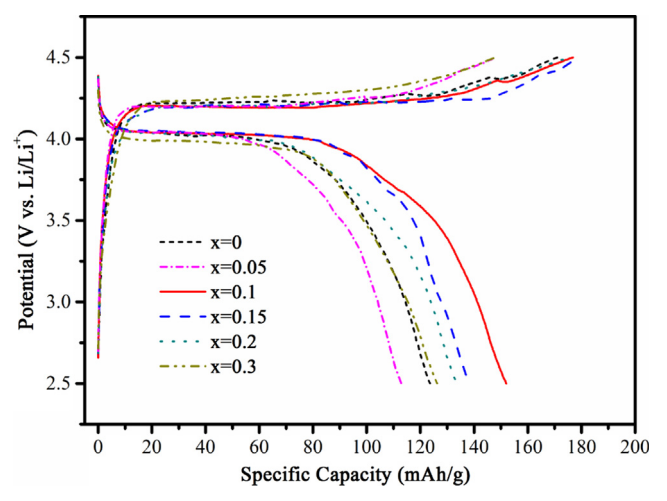


Fig. 6. First charge-discharge curves of  ${\rm Li_{1-x}Na_xMnPO_4/C}$  (x = 0, 0.05, 0.1, 0.15, 0.2, 0.3) at 0.05 C.

The cycling performance and rate capabilities of all the samples are also measured to evaluate the electrochemcial activity of the cathode materials. The cycling performance of  $Li_{1-x}Na_xMnPO_4/C$  (x = 0, 0.05, 0.1, 0.15, 0.2, 0.3) composites are tested at 0.05 C for over 200 cycles, and the results are shown in Fig. 7a. After 200 cycles at 0.05 C, the specific discharge capacity of Li<sub>0.9</sub>Na<sub>0.1</sub>MnPO<sub>4</sub>/C electrode remains at 142.5 mAh/g with only 6.2% capacity loss, which is advantage over other doped samples, indicating the proper adding amounts of sodium ions could maintain the chemical and structural stability of the cathode material during the insertion and extraction process for lithium ions. The representative rate capabilities of all samples are evaluated at 0.05-1 C discharge rates under room temperature, and the plots are presented in Fig. 7b. As the discharge rates increase from 0.05 C to 1 C, the specific capacities of all samples present a serious downward trend, in which the specific capacity of Li<sub>0.9</sub>Na<sub>0.1</sub>MnPO<sub>4</sub>/C electrode decreases gradually and keeps more stable. It is observed that Li<sub>0.9</sub>Na<sub>0.1</sub>MnPO<sub>4</sub>/C delivers the relative lower rate decays with the discharge capacities of 152 mAh/g, 150.2 mAh/g, 147.1 mAh/g, 145.1 mAh/g, 142.3 mAh/g and 122.3 mAh/g at 0.05 C, 0.1 C, 0.2 C, 0.5 C, 1 C and 10 C in order. In contrast to the low rate of 0.05 C, the rate capacity is still high at higher

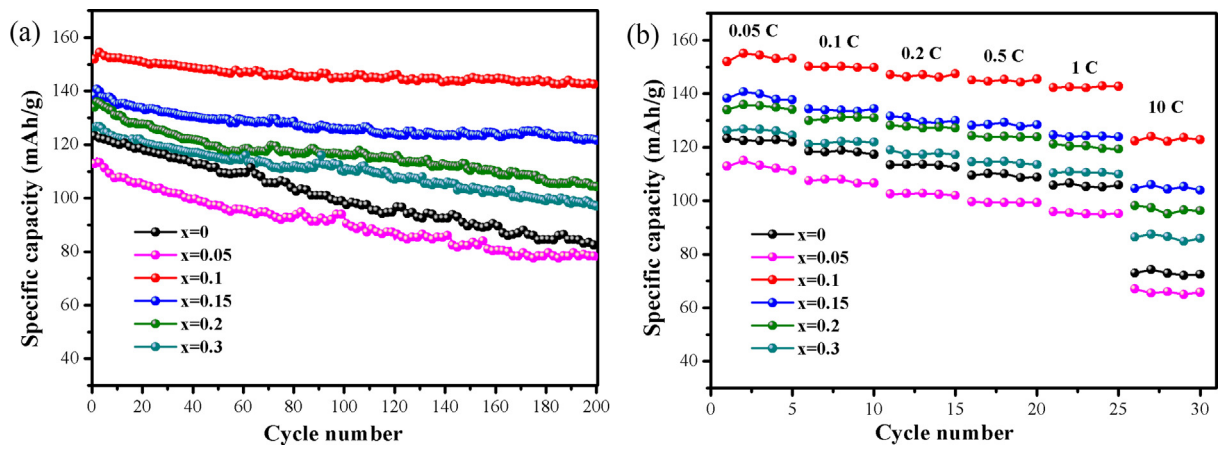


Fig. 7. Electrochemical performance of  $\text{Li}_{1-x}\text{Na}_x\text{MnPO}_4/\text{C}$  (x = 0, 0.05, 0.1, 0.15, 0.2, 0.3): (a) The cycling performance, (b) The rate capabilities.

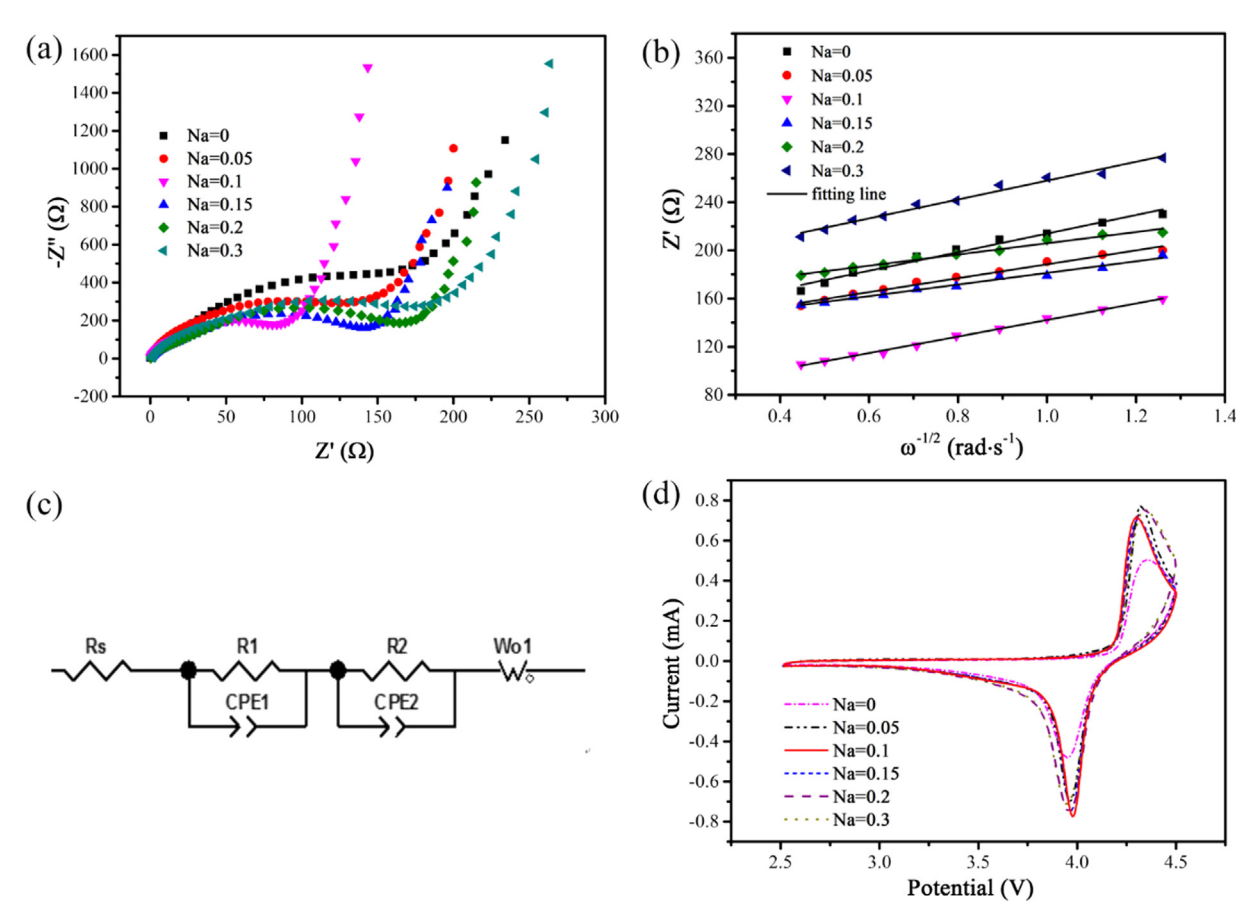


Fig. 8. Li<sub>1-x</sub>Na<sub>x</sub>MnPO<sub>4</sub>/C (x = 0, 0.05, 0.1, 0.15, 0.2, 0.3) samples: (a) EIS plots; (b) The liner fitting line between Z' and  $w^{-1/2}$  at low-frequency region; (c) Equivalent circuit; (d) CV curves.

discharge rate, which shows better high rate discharge performance. With the discharge rates increasing, the intercalation/deintercalation rate of Li  $^{\rm +}$  in the bulk material accelerates, and thus improves the Li ion diffusion rate in the channels.

To further understand the reaction kinetics of Li<sub>1-x</sub>Na<sub>x</sub>MnPO<sub>4</sub>/C (x = 0, 0.05, 0.1, 0.15, 0.2, 0.3) composites, the electrochemical impedance spectroscopy (EIS) and cyclic voltammetry (CV) are conducted, and the results are shown in Fig. 8. Fig. 8a shows the EIS spectrum of  $\text{Li}_{1-x}\text{Na}_x\text{MnPO}_4/\text{C}$  (x = 0, 0.05, 0.1, 0.15, 0.2, 0.3) electrodes in the frequency range of 10<sup>5</sup> Hz-0.1 Hz. The spectra include a semicircle in the high-frequency and a sloping line in the low-frequency range, which are attributed to complex charge transfer resistance between the electrolyte and the active material through the solid electrolyte interface formed on the electrodes surface (R<sub>SEI</sub>, R<sub>ct</sub>) and the lithium ions diffusion rate (Wo), respectively. It is evident that Li<sub>0.9</sub>Na<sub>0.1</sub>MnPO<sub>4</sub>/C electrode has the smallest circle diameter, indicating that Li<sub>0.9</sub>Na<sub>0.1</sub>MnPO<sub>4</sub>/C delivers the lowest charge transfer resistance, which could ascribed to the improved ionic conductivity and be one of the main reasons of the improved discharge capacity. In order to further analyze the effect of lithium-sodium ratio on the charge transfer dynamics, the EIS results are fitted, the linear fitting curves between Z' and  $w^{-1/2}$  and the equivalent circuit diagram are represented in Fig. 8b and c. In the model, Rs is the solution resistance, R1 and R2 corresponds to the surface film resistance (RSEI) and the charge transfer process resistance (Rct) in the complex interface. The studied sodium doped LiMnPO<sub>4</sub>/C composites consist of multiple interfaces and phase boundaries, and the relevant impedance analysis are complicated. Furthermore, the lithium-ion diffusion coefficient  $\left(D_{Li}^{\phantom{Li}+}\right)$  can be calculated for all the sodium doped LiMnPO<sub>4</sub>/C composite samples by following equation  $D_{Li^+} = R^2 T^2 / 2A^2 n^4 F^4 C^2 \sigma^2$  $Z' = R_s + R_{ct} + \sigma w^{-1/2}$ , where R, T, A, n, F and C are the gas constant,

absolute temperature, efficient surface area, the number of electrons per molecule, Faraday constant and the concentration of lithium ion, respectively. Accordingly, the Warburg factor ( $\sigma$ ) is the slope of the graph between Z' and reciprocal square root of the angular frequency at low-frequency region (Fig. 8b), and is proportional to the lithium ion diffusion coefficient. Although the lithium ions diffusion coefficient of  $\text{Li}_{0.9}\text{Na}_{0.1}\text{MnPO}_4/\text{C}$  cathode is not the maximum, but it shows the minimum  $R_{ct}$  value. Presuasively, it is reasonable that  $\text{Li}_{0.9}\text{Na}_{0.1}\text{MnPO}_4/\text{C}$  has tremendous advantages for efficient charge storage properties. Based on the above analysis, the adding ratio of sodium has a crucial influence on the kinetics of  $\text{Li}_{1-x}\text{Na}_x\text{MnPO}_4/\text{C}$ , and a suitable sodium ratio can effectively improve its electrical conductivity and reduce the charge transfer resistance in the electrochemical cycling process, resulting in superior lithium storage performance.

Fig. 8d compares the CV plots of all the samples with a sweeping rate of 0.1 mV/s in the voltage range of 2.5–4.5 V (vs. Li $^+$ /Li). A couple of good symmetry oxidation/reduction peaks is observed, which correspond to Mn<sup>3+</sup>/Mn<sup>2+</sup> redox reaction coupled with the insertion/deinsertion process of the lithium ions, and also indicate that it is a quasi-reversible reaction. It is obviously observed that the voltage difference value between the oxidation and reduction peaks of Li<sub>0.9</sub>Na<sub>0.1</sub>MnPO<sub>4</sub>/C is close to 0.31 V, far below the value of other samples, indicating the excellent reaction process kinetics and slight electrochemical polarization of the bulk material due to the enhanced electronic and ionic conductivity. With the sodium ions adding amounts increasing, the potential interval expands and polarization phenomenon becomes serious, indicating a certain content of sodium ions is favorable to improving the reversibility and decreasing polarization of pure LiMnPO<sub>4</sub>/C.

#### 4. Conclusions

Sodium ions have been successfully doped at Li site and embedded into the lattice of LiMnPO $_4$  via a normal hydrothermal routine. The proper adding amounts of sodium ions are beneficial to refine crystal size, improve monodispersity, increase the electrical conductivity, and improve the mobility of lithium ions. Compared with other samples, Li $_{0.9}$ Na $_{0.1}$ MnPO $_4$ /C electrode delivers the highest initial discharge capability of 152 mAh/g at 0.05 C and 122.3 mAh/g at 10 C, which also shows excellent rate performance. In conclusion, sodium doping at Li site is an efficient approach to widen the lithium ions diffusion path and further improve the conductivity of LiMnPO $_4$ /C, which is favour of large-scale application.

#### CRediT authorship contribution statement

Jun Zhang: Conceptualization, Methodology, Writing - original draft, Software. Shao-Hua Luo: Supervision, Resources. Qun-Xiang Ren: Visualization, Investigation, Supervision, Resources. Da-Jun Zhang: Data curation, Software. Yan Qin: Validation, Formal analysis.

#### **Declaration of Competing Interest**

The authors declare that they have no known competing financial interests or personal relationships that could have appeared to influence the work reported in this paper.

#### Acknowledgments

This work was financially supported by the National Natural Science Foundation of China (No. 51674068, 51704064, 51874079, 51804035), Natural Science Foundation of Hebei Province (No. E2018501091), The Training Foundation for Scientific Research of Talents Project, Hebei Province (No. A2016005004), Hebei Province higher education science and technology research project (No. QN2017403). The Fundamental Research Funds for the Central Universities (No. N172302001, N182312007, N182304015). Qinhuangdao City University student of Science and Technology Innovation and Entrepreneurship Project (No. PZB1810008T-46, PZB1810008T-14), The Doctoral Scientific Research Foundation of Shenyang Medical College (No. 20195076).

#### References

- [1] S.K. Zhong, L. Wu, J. Liu, Sol–gel synthesis and electrochemical properties of 9LiFePO<sub>4</sub>·Li<sub>3</sub>V<sub>2</sub>(PO<sub>4</sub>)<sub>3</sub>/C composite cathode material for lithium ion batteries, Electrochim. Acta 74 (2012) 8–15.
- [2] S.H. Luo, Z.L. Tang, J.B. Lu, Z.T. Zhang, Electrochemical properties of carbon-mixed LiFePO<sub>4</sub> cathode material synthesized by the ceramic granulation method, Ceram. Int. 34 (2008) 1349–1351.
- [3] S.K. Martha, B. Markovsky, J. Grinblat, LiMnPO<sub>4</sub> as an advanced cathode material for rechargeable lithium batteries, J. Electrochem. Soc. 156 (2009) A541–A552.
- [4] S. Luo, D. Hu, H. Liu, J. Li, T.F. Yi, Hydrothermal synthesis and characterization of α-Fe<sub>2</sub>O<sub>3</sub>/C using acid pickled iron oxide red for Li-ion batteries, J. Hazard. Mater. 368 (2019) 714–721.
- [5] S. Bao, S. Luo, S. Yan, Z. Wang, Q. Wang, J. Feng, Y. Wang, T. Yi, Nano-sized MoO<sub>2</sub> spheres interspersed three-dimensional porous carbon composite as advanced anode for reversible sodium/potassium ion storage, Electrochim. Acta 307 (2019) 293–301.
- [6] S. Luo, Y. Sun, S. Bao, J. Li, J. Zhang, T.F. Yi, Synthesis of Er-doped LiMnPO<sub>4</sub>/C by a sol-assisted hydrothermal process with superior rate capability, J. Electroanal. Chem. 832 (2019) 196–203.
- [7] H. Liu, S. Luo, D. Hu, X. Liu, Q. Wang, Z. Wang, Y. Wang, L. Chang, Y. Liu, T.F. Yi, Y. Zhang, A. Hao, Design and synthesis of carbon-coated  $\alpha$ -Fe<sub>2</sub>O<sub>3</sub>@Fe<sub>3</sub>O<sub>4</sub> heterostructured as anode materials for lithium ion batteries, Appl. Surf. Sci. 495 (2019) 143590.
- [8] L. Liang, X. Sun, J. Zhang, et al., In situ synthesis of hierarchical core double-shell Ti-doped LiMnPO<sub>4</sub>@NaTi<sub>2</sub>(PO<sub>4</sub>)<sub>3</sub>@C/3D graphene cathode with high-rate capability and long cycle life for lithium-ion batteries, Adv. Energy Mater. 9 (11) (2019) 1802847.

- [9] J. Li, S. Luo, Q. Wang, et al., Facile synthesis of carbon-LiMnPO<sub>4</sub> nanorods with hierarchical architecture as a cathode for high-performance Li-ion batteries, Electrochim. Acta 289 (2018) 415–421.
- [10] S.K. Kumar, S.K. Martha, Li<sub>1.2</sub>Mn<sub>0.55</sub>Ni<sub>0.15</sub>Co<sub>0.1</sub>O<sub>2</sub>(LMR-NMC)-carbon coated-LiMnPO<sub>4</sub> blended electrodes for high performance lithium ion batteries, J. Electrochem. Soc. 165 (3) (2018) A463–A468.
- [11] L. Esmezjan, D. Mikhailova, M. Etter, et al., Electrochemcal lithium extraction and insertion process of sol-gel synthesized LiMnPO<sub>4</sub> via two-phase mechanism, J. Electrochem. Soc. 166 (6) (2019) A1257–A1265.
- [12] I. Bezza, M. Kaus, R. Heinzmann, Mechanism of the delithiation/lithiation process in LiFe $_0$ . 4M $_{n0}$ ,6P $_0$ 4: in situ and ex situ investigations on long-range and local structures, J. Phys. Chem. C 119 (2015) 9016–9024.
- [13] V. Ragupathi, P. Panigrahi, G.S. Nagarajan, Enhanced electrochemical performance of nanopyramid-like LiMnPO<sub>4</sub>/C cathode for lithium-ion batteries, Appl. Surf. Sci. 495 (2019) 143541.
- [14] X. Pan, Z. Gao, L. Liu, et al., Self-templating preparation and electrochemical performance of LiMnPO<sub>4</sub> hollow microspheres, J. Alloy. Compd. 783 (2019) 468–477.
- [15] N.H. Kwon, H. Yin, T. Vavrova, et al., Nanoparticle shapes of LiMnPO<sub>4</sub>, Li<sup>+</sup> diffusion orientation and diffusion coefficients for high volumetric energy Li<sup>+</sup> ion cathode, J. Powder Sources 342 (2017) 231–240.
- [16] L. Wang, H. Zhang, Q. Liu, et al., Modifying high-voltage olivine-type LiMnPO<sub>4</sub> cathode via Mg substitution in high-orientation crystal, ACS Appl. Energy Mater. 1 (11) (2018) 5928–5935.
- [17] A. Gutierrez, R. Qiao, L. Wang, High-capacity, aliovalently doped olivine LiMn<sub>1-3x/</sub> 2V<sub>x□x/2</sub>PO<sub>4</sub> cathodes without carbon coating, Chem. Mater. 26 (9) (2014) 3018–3026
- [18] F.A. Vasquez, J.A. Calderon, Vanadium doping of LiMnPO<sub>4</sub> cathode material: Correlation between changes in the material lattice and the enhancement of the electrochemcial performance, Electrochim. Acta 325 (2019) 134930.
- [19] R.E. Khalfaouy, A. Addaou, A. Laajeb, Synthesis and characterization of Na-substituted LiMnPO<sub>4</sub> as a cathode material for improved lithium ion batteries, J. Alloy. Compd. 775 (2019) 836–844.
- [20] Y.R. Zhu, R. Zhang, L. Deng, T.F. Yi, Lithium-ion insertion kinetics of Na-doped LiFePO<sub>4</sub> as cathode materials for lithium-ion batteries, Metall. Mater. Trans. E 2 (1) (2015) 33–38.
- [21] K. Rajammal, D. Sivakumar, Na-doped LiMnPO<sub>4</sub> as an electrode material for enhanced lithium ion batteries. Bull. Mater. Sci. 40 (1) (2017) 171–175.
- [22] W. Chen, H. Fang, Communication-Aluminum doping in LiMnPO<sub>4</sub> with an unexpected charge compensation, J. Electrochem. Soc. 166 (13) (2019) A2752–A2754.
- [23] J. Zhang, S. Luo, L. Sui, Co-precipitation assisted hydrothermal method to synthesize Li<sub>0.9</sub>Na<sub>0.1</sub>Mn<sub>0.9</sub>Ni<sub>0.1</sub>PO<sub>4</sub>/C nanocomposite as cathode for lithium ion battery, J. Alloy. Compd. 768 (2018) 991–994.
- [24] J. Zhang, S. Luo, Q. Wang, Yttrium doping at Mn-site to improve electrochemical kinetics activity of sol-gel synthesized LiMnPO<sub>4</sub>/C as cathode for lithium ion battery, J. Solid State Electr. 21 (11) (2017) 3189–3194.
- [25] J. Zhang, S. Luo, L. Chang, In-situ growth of LiMnPO<sub>4</sub> on porous LiAlO<sub>2</sub> nanoplates substrates from AAO synthesized by hydrothermal reaction with improved electrochemical performance, Electrochim. Acta 193 (2016) 16–23.
- [26] H.C. Dinh, S. Mho, Y. Kang, et al., Large discharge capacities at high current rates for carbon-coated LiMnPO<sub>4</sub> nanocrystalline cathodes, J. Powder Sources 244 (2013) 189–195.
- [27] Z. Xie, K. Chang, B. Li, et al., Glucose-assisted synthesis of highly dispersed LiMnPO<sub>4</sub> nanoparticles at a low temperature for lithium ion batteries, Electrochim. Acta 189 (2016) 205–214.
- [28] C. Ouyang, S. Shi, Z. Wang, First-principles study of Li ion diffusion in LiFePO<sub>4</sub>, Phys. Rev. B 69 (10) (2004) 104303.
- [29] D. Morgan, A. Van der Ven, G. Ceder, Li conductivity in LixMPO4 (M = Mn, Fe Co, Ni) olivine materials, Electrochem. Solid ST 7 (2) (2004) A30–A32.
- [30] C.Y. Ouyang, D.Y. Wang, S.Q. Shi, First principles study on  $Na_x Li_{1-x} FePO_4$  as cathode material for rechargeable lithium batteries, Chinese Phys. Lett. 23 (1) (2006) 61.
- [31] X.G. Yin, K.L. Huang, S.Q. Liu, Preparation and characterization of Na-doped LiFePO<sub>4</sub>/C composites as cathode materials for lithium-ion batteries, J. Power Sources 195 (2010) 4308–4312.
- [32] M.M. Jia, Y.H. Zhang, H.L. Tian, Z. Su, Synthesis and electrochemical performance of Na<sub>3-x</sub>Li<sub>x</sub>V<sub>2</sub>(PO<sub>4</sub>)<sub>3</sub>/C as cathode materials for Li-ion batteries, Int. J. Energy Res. 43 (11) (2019) 1–9.
- [33] Z.L. Zuo, J.Q. Deng, J. Pan, High energy density of Li<sub>3.x</sub>Na<sub>x</sub>V<sub>2</sub>(PO<sub>4</sub>)<sub>3</sub>/C cathode material with high rate cycling performance for lithium-ion batteries, J. Power Sources 357 (2017) 117–125.
- [34] X.D. Yan, L.Q. Xin, H. Wang, Synergetic effect of Na-doping and carbon coating on the electrochemcial performances of Li<sub>3-x</sub>Na<sub>x</sub>V<sub>2</sub>(PO<sub>4</sub>)<sub>3</sub>/C as cathode for lithium-ion batteries, RSC Adv. 9 (2019) 8222–8229.
- [35] Q. Kuang, Y. Zhao, Z. Liang, Synthesis and electrochemical properties of Na-doped Li<sub>3</sub>V<sub>2</sub>(PO<sub>4</sub>)<sub>3</sub> cathode materials for Li-ion batteries, J. Power Sources 196 (23) (2011) 10169–10175.
- [36] Y.R. Zhu, R. Zhang, L. Deng, T.F. Yi, Lithium-ion insertion kinetics of Na-doped LiFePO<sub>4</sub> as cathode materials for lithium-ion batteries, Metall. Mater. Trans. E 2 (1) (2015) 33–38.
- [37] J. Zhang, S.H. Luo, Q. Wang, Z.Y. Wang, A.M. Hao, Optimized hydrothermal synthesis and electrochemical performance of LiMnPO<sub>4</sub>/C cathode materials using high specific area spherical structure Li<sub>3</sub>PO<sub>4</sub>, J. Alloy. Compd. 701 (2017) 433–438.